Chapter 6 -- Parametric Studies / Design Considerations

6.1 Overview

The numerical analysis technique described in Chapter Four of this work has been applied for solution of the linear and geometrically nonlinear equations of shell theory developed in Chapters Two and Three, and the results have been tested for correctness by the tests reported in Chapter Five, and by the tests described in Steinbrink and Johnson (1997), along with many other unreported tests. There is therefore ample reason to believe that a reliable analysis has been constructed. In this chapter, that analysis is used to examine the responses of various domes used to close a specified test cylinder. For all of these analyses, the test cylinder is taken to have a fixed design. For most analyses, the cover plate used to close the polar opening of the dome is also of fixed design; the only parameters to be varied are thus parameters of the dome. Specifically, the shape of the meridian and the laminate properties of the dome will be varied. After the results of these parametric studies are described, some attention is given to the effect of cover plate design on the overall structural response

There are, of course, a large number of possible dome geometries which may sometimes be appropriate for closure of the cylinder, and an infinite number of possible material systems and laminates which might be chosen. In order to maintain a manageable number of design permutations, we will consider only unstiffened, eight-ply ellipsoidal domes. We begin with an investigation of quasi-isotropic laminates, and proceed to choose laminate layups for subsequent analyses based upon the results obtained for the quasi-isotropic case.

6.1.1 Material properties

One goal of this chapter is to provide a useful set of data for comparison to physical tests which may be performed in the future. With this goal in mind, a single material system is chosen, having "real" material properties. Note that this is in contrast to the studies of Chapter Five, which were for numerical verification only. For the purpose of this study, we choose the following material properties, which are representative of AS4/3502 polymer matrix composite material: E_1 = 19.63 Msi, E_2 = 1.46 Msi, $G_{12} = G_{13}$ = 0.82 Msi, ν_{12} = 0.295, and G_{23} = 0.683 Msi.

These values were taken in consultation with Dr. James Starnes, Jr., Branch Head of the Structural Mechanics Branch of NASA Langley Research Center, except for the value of G_{23}, which was estimated by finite element analysis of a transverse shear deformable cylinder.

We assume an ultimate stress (tensile or compressive) for the fibers given by $\sigma_u = 2(10^5)psi$, and lamina thickness of 0.005 inches. These material properties are used for both the cylinder and the dome. The cover plate and the stiffening ring at the cylinder/dome joint are assumed to be constructed of Titanium alloy (isotropic), having the material properties

$$E = 15Msi \qquad \nu = 0.34 .$$

6.1.2 Cylinder/dome/cover plate design

The cylinder is assumed for this work to have a fixed design, specifically, that of a right circular cylinder with 12" radius, and a quasi-isotropic $[\pm 45,0,90]_s$ layup. The cover plate is initially taken to be of 0.04" thick Titanium alloy, with a radius of 3 inches. There is a strap-type stiffening ring at the cylinder/dome interface, which is modeled as a point stiffener along the meridian, with "stiffness" $E \cdot Area$. The ring is 1/8" thick Titanium alloy, with a length along the cylinder meridian of 1.5 inches. The total configuration is as shown in Fig. 6.1. There are 3/4" overlaps between the cylinder and dome and between the cover plate and dome, which are assumed to have negligible stiffness relative to the strap and plate, and are ignored.

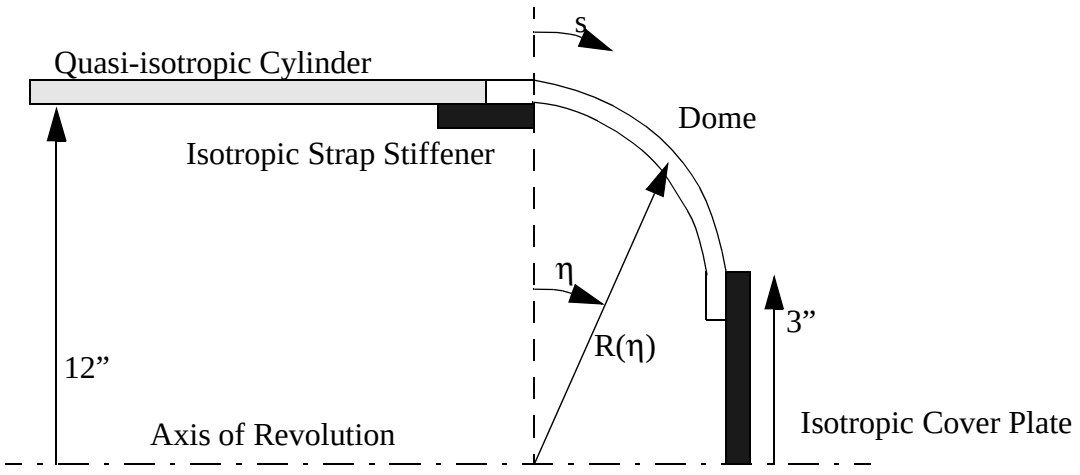

Fig. 6.1 Assumed Geometry of Test Specimens

The cylinder and cover plate are not modeled in the multiple shooting analysis whose results are described here. Instead, the two peripheral structures are treated as equivalent sets of linear elastic springs, as detailed in Section 3.5. The elastic stiffness matrices and fixed-end vectors are given in equation (6.1), below. The elastic stiffnesses for the cylinder were calculated using the multiple shooting code, and the elastic stiffnesses for the cover plate were taken from linear plate theory for a circular flat plate (Baker, Kovalesky and Rish, 1981, pages 141-51). It is assumed that the plate will not resist circumferential motion, normal motion, or rotation about the meridional axis. The correspondent stiffnesses are thus set to zero in the K_{plate} matrix of equation (6.1). It may be noted that the stiffness matrix for the cylinder is not perfectly symmetric. This is a pitfall of the numerical approximation technique used to calculate it -- numerical error causes some inaccuracy. The asymmetry is slight, and is ignored for this work; such asymmetry also was seen in the stiffness matrices used for the verification studies of section 5.2. For that work, the inaccuracy did not seem to adversely affect the solution, and the shooting and finite element results agreed nicely.

$$K_{cyl} = \begin{bmatrix} 14080 & 0.0 & 0.9404 & -1.5780 & -0.2653 \\ 0.0 & 4294 & 0.0 & 0.0 & -0.4935 \\ 0.9406 & 0.0 & 19530 & 1.9325 & 0.3193 \\ -1.5776 & 0.0 & 1.9324 & 13.586 & 2.2498 \\ -0.2652 & -0.4935 & 0.3196 & 2.2498 & 834.8 \end{bmatrix} \qquad \textbf{(6.1)}$$

$$v_{cyl} = [3.5621,\ 0.246\times10^{-2},\ -0.2798,\ -0.4342\times10^{-1},\ -0.7097\times10^{-2}]$$

$$K_{plate} = \begin{bmatrix} 303000 & 0.0 & 0.0 & 0.0 & 0.0 \\ 0.0 & 0.0 & 0.0 & 0.0 & 0.0 \\ 0.0 & 0.0 & 0.0 & 0.0 & 0.0 \\ 0.0 & 0.0 & 0.0 & 26.27 & 0.0 \\ 0.0 & 0.0 & 0.0 & 0.0 & 0.0 \end{bmatrix}$$

$$v_{plate} = [0.0,\ 0.0,\ -1.5,\ -0.1217,\ 0.0]$$

The equivalent elastic stiffnesses and fixed-end vector of the cylinder are determined under the assumption that the "remote" end of the cylinder (that is, the end away from the dome) experiences a membrane response. Such will likely be the case if the test specimen is a long cyl-

inder capped by identical domes on each end. In that case, the remote end of the cylinder in the model for the shooting analysis corresponds to the center point along the meridian of the test cylinder. The model depicted in Fig.6.1 is thus in effect a half-symmetry model of the entire meridian.

The loading on the shell is internal hydrostatic pressure only, with magnitude $p = 55$ psi. This pressure provides an average membrane circumferential stress in the cylinder of 16,500 psi, which is thought to be roughly equivalent to the design load on a full-sized aircraft fuselage.

We begin this parametric study with an examination of quasi-isotropic ellipsoidal domes. Specifically, we will look at $[\pm 45,0,90]_s$ laminates. Reiterating from Chapter 5, the ellipticity of the meridian is defined as the ratio of the axis length parallel to the axis of revolution to the axis length normal to the axis of revolution, so that spherical domes have ellipticity $e = 1.0$. We are also interested only in low-weight domes, so we take $0 < e \leq 1.0$, where a lower value of e corresponds to a dome which is more flat -- ellipticity $e = 0.0$ would correspond to a flat plate normal to the axis of revolution. Following this study of quasi-isotropic ellipsoids, we will look at ellipsoids with different laminate properties.

6.1.3 Criteria for judgement of dome fitness

The dome designs considered will be judged against one another based on a minimum weight criterion, subject to stability and material failure constraints. Material failure will be considered only for the fibers, using a maximum stress approach. If the fiber-direction stress in any ply of the dome exceeds fiber ultimate strength (tensile or compressive) at any location, then the dome is judged to have failed. Stability has not been encoded into the current analysis, but it is assumed that the dome will not buckle unless one or both in-plane normal stress resultants N_{11}, N_{22} (Figs. 3.1, 3.2) is compressive. For the purpose of this parametric study, a design is considered to be undesirable if either N_{11} or N_{22} is negative at any location.

Weight of the dome is not actually calculated, but an approximate dome material volume is found, and used as a basis for comparison. The algorithm for computation of material volume is as follows. Arc length position of all shooting points is determined by integration of the merid-

ional surface metric along the meridian. The approximate differential volume between shooting points is then found by multiplying the length of arc between two adjacent shooting points by $2\pi Rt$, where R is the shortest distance from the midpoint of the shooting segment to the axis of revolution, and t is the (constant) shell thickness. Total approximate volume is found by summing the differential volumes. Inasmuch as the domes being compared are all of the same material, lower volume must correspond to lower weight.

6.2 Quasi-isotropic ellipsoidal domes

The examination of quasi-isotropic ellipsoidal domes was performed sequentially, beginning with a spherical dome, and proceeding in steps to increase the ellipticity (i.e., reduce e) of the dome on subsequent analyses. The following general trends were noted.

The response of the spherical dome included a significant boundary layer effect at the joint with the cover plate, as may be expected given the material and geometric discontinuities which exist at that location. Similar boundary layer effects are seen near the cylinder/dome interface for all primary response quantities except meridional displacement u, meridional stress resultant N_{11}, and circumferential displacement v. A boundary layer effect is not seen for these variables at the cylinder/dome joint because there exists no material discontinuity in the meridional direction at that location and the geometric discontinuity is small -- the tangent to the meridian is continuous. Although the values of the dependent variables are affected by dome ellipticity, the presence of a boundary layer does not seem to be -- no increase in ellipticity results in elimination of the boundary layer effects. It thus seems that such boundary layer effects as occur are primarily driven by material discontinuity at the dome/cover plate junction.

For the spherical dome, there exists a small compressive circumferential stress resultant N_{22} near the cover plate which is relieved by adjustment of the geometry. Refer to Figure 6.2. Increasing ellipticity causes the compressive magnitude of N_{22} to be reduced, and N_{22} becomes tensile for an ellipticity somewhere between $e = 0.85$ and $e = 0.80$. At this point, a state of uniform biaxial tension exists in the dome, thus relieving any worries we might have had regarding shell elastic stability. At the same time, the magnitude of N_{22} is reduced in the vicinity of the cylinder/dome joint, becoming less tensile, until a compressive state is again reached for $e = 0.73$.

For higher ellipticity, the quality of the response deteriorates rapidly, in the sense that compressive N_{22} becomes large, and boundary layer effects are generally made more severe. There seems to exist, then, a "best" range of ellipticities for the dome to avoid hoopwise compression. At no value of ellipticity was fiber failure seen to be a concern.

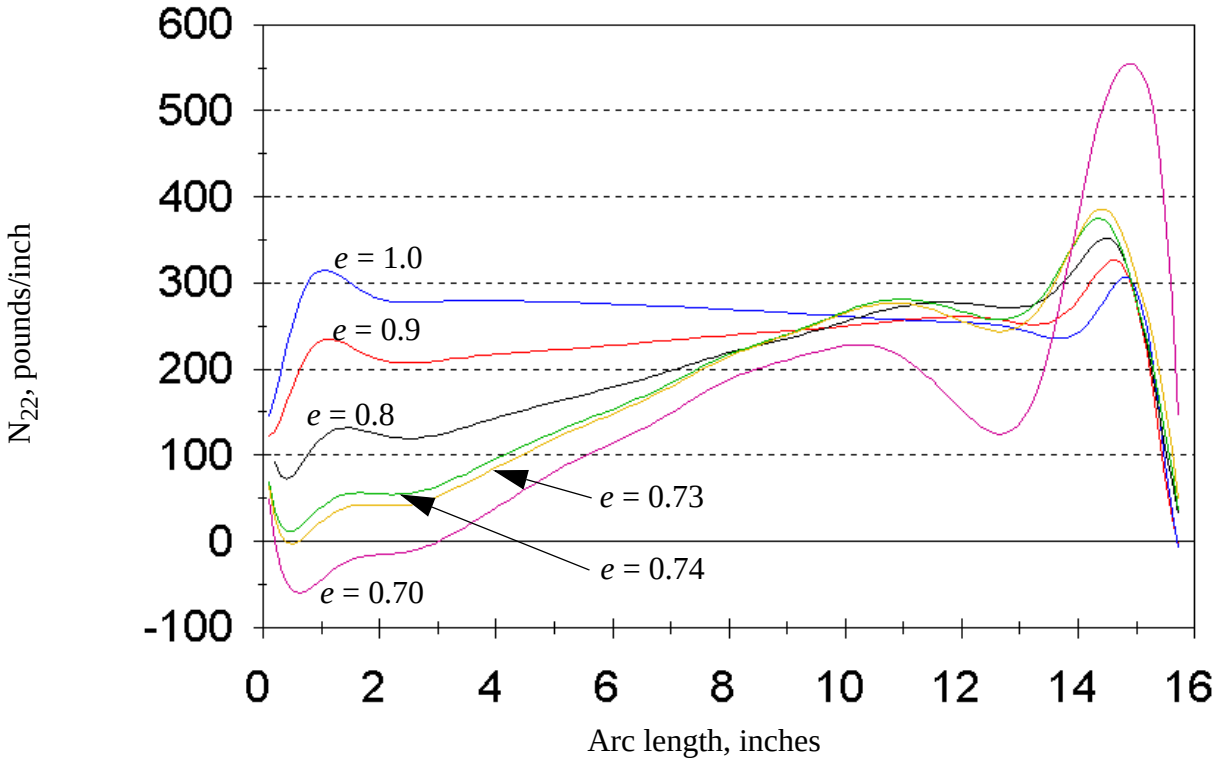

Fig. 6.2 Circumferential Stress Resultant for Various Ellipticities, Quasi-isotropic Dome

It may be interesting to note that the meridional stress resultant N_{11} is affected by dome ellipticity in just the same way as is the circumferential stress resultant N_{22} -- increased ellipticity results in reduced tensile stress resultant in the vicinity of the cylinder, and increased tensile stress resultant in the vicinity of the cover plate. Refer to Fig. 6.3. Again, note that the response for ellipticity $e = 0.70$ is very different from the responses for larger values of e, indicating the onset of some numerical phenomenon, possibly limit-point buckling. This is consistent with the results

discussed above and shown in Fig. 6.2, and will be further discussed at the end of this section.

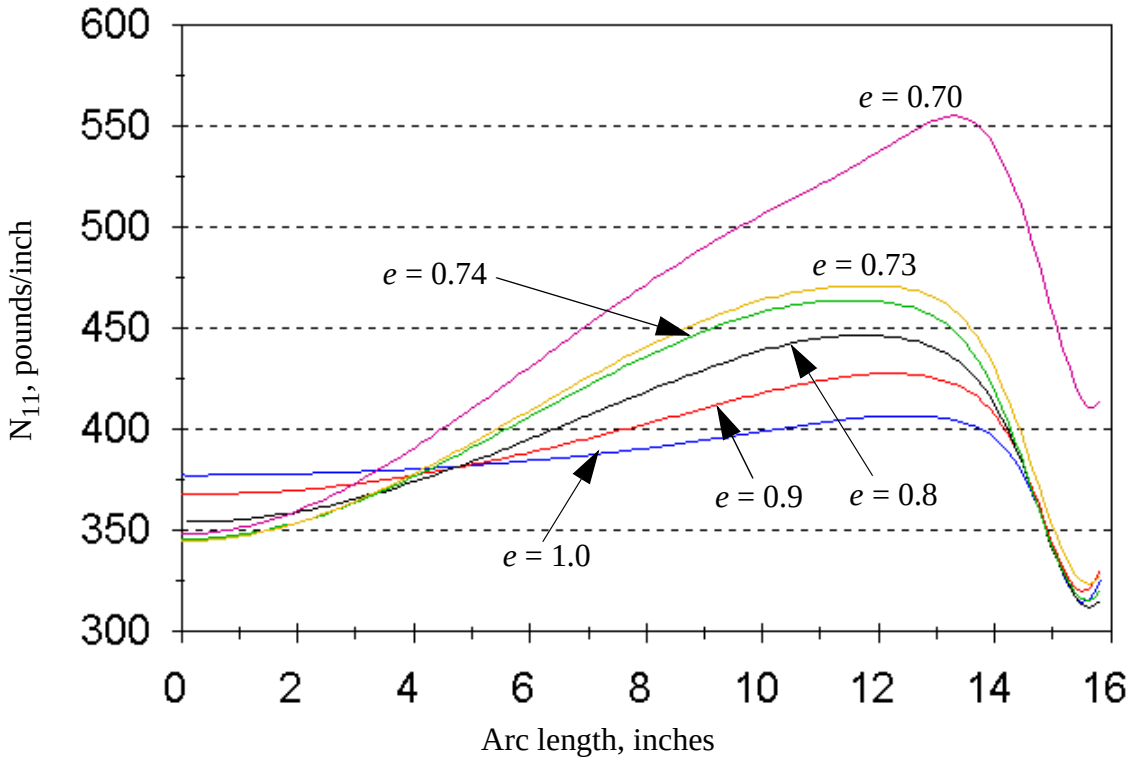

Fig. 6.3 Meridional Stress Resultant for Various Ellipticities, Quasi-isotropic Dome

On the basis of the results already given for the circumferential stress resultant N_{22}, it seems that the "best" design for the quasi-isotropic dome is that which has ellipticity defined by $e = 0.74$. Results for the significant displacements and stress resultants are shown in Figs. 6.4-6.14, for the spherical dome ($e = 1.0$) and for $e = 0.74$. It may be seen that the overall response of the dome is somewhat more severe for the non-spherical dome, but not grossly so. In particular, the two results for the rotation about the meridional axis, ϕ_2, are so close to one another as to be almost indistinguishable. Refer to Fig. 6.8. The approximate material volume of the spherical dome is 35.0 cubic inches, and the approximate volume of the "best" dome is 29.0 cubic inches. The relative weight savings is thus approximately 17% in the move from spherical to "best" geometry.

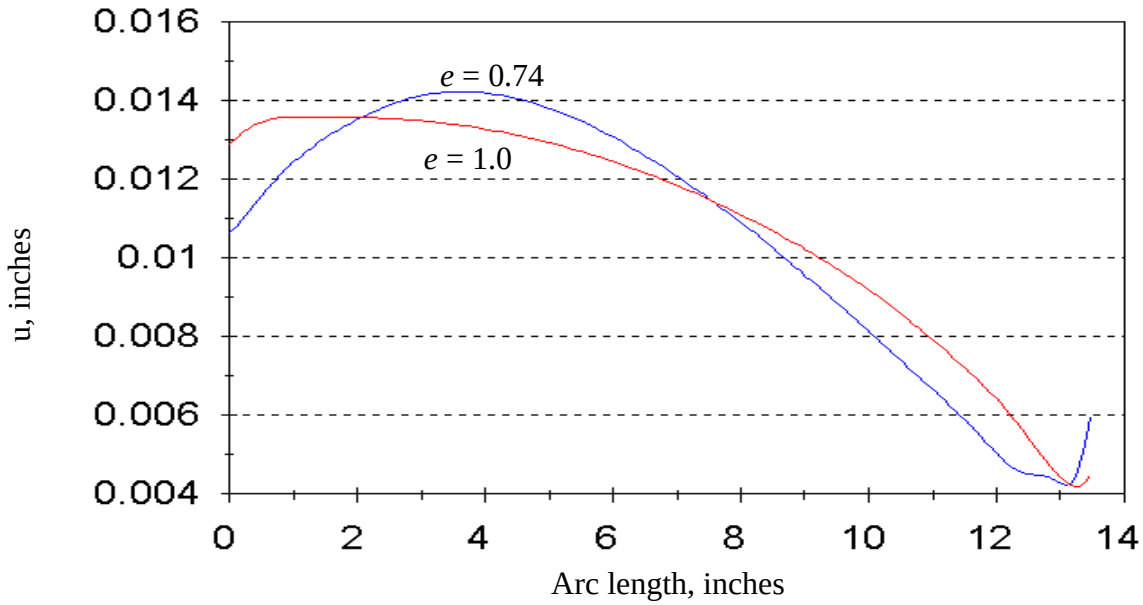

Fig. 6.4 Meridional Displacement, Quasi-isotropic Dome

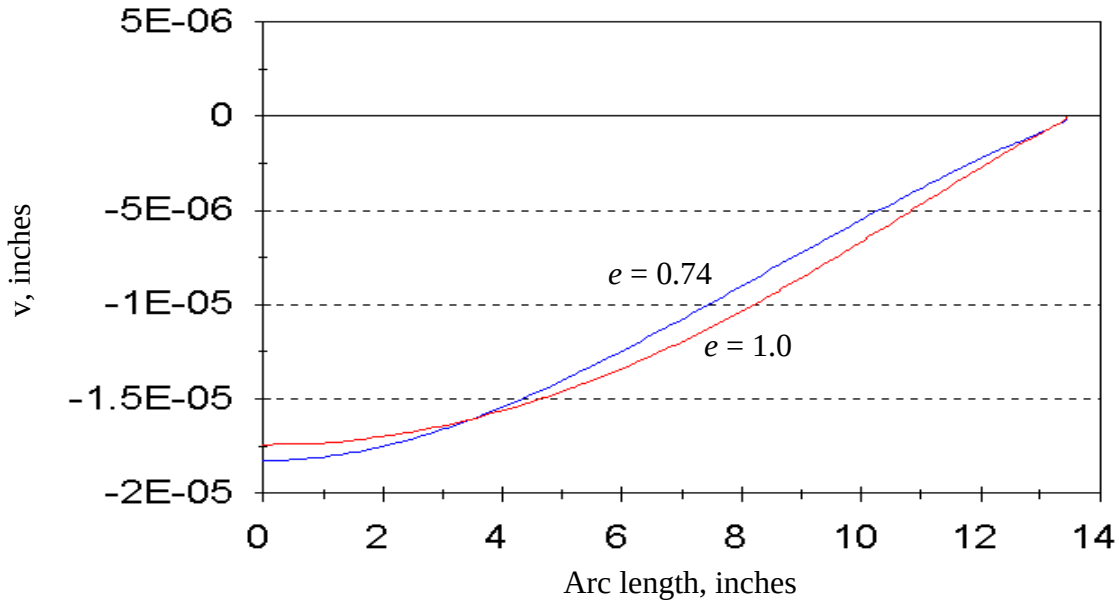

Fig. 6.5 Circumferential Displacement, Quasi-isotropic Dome

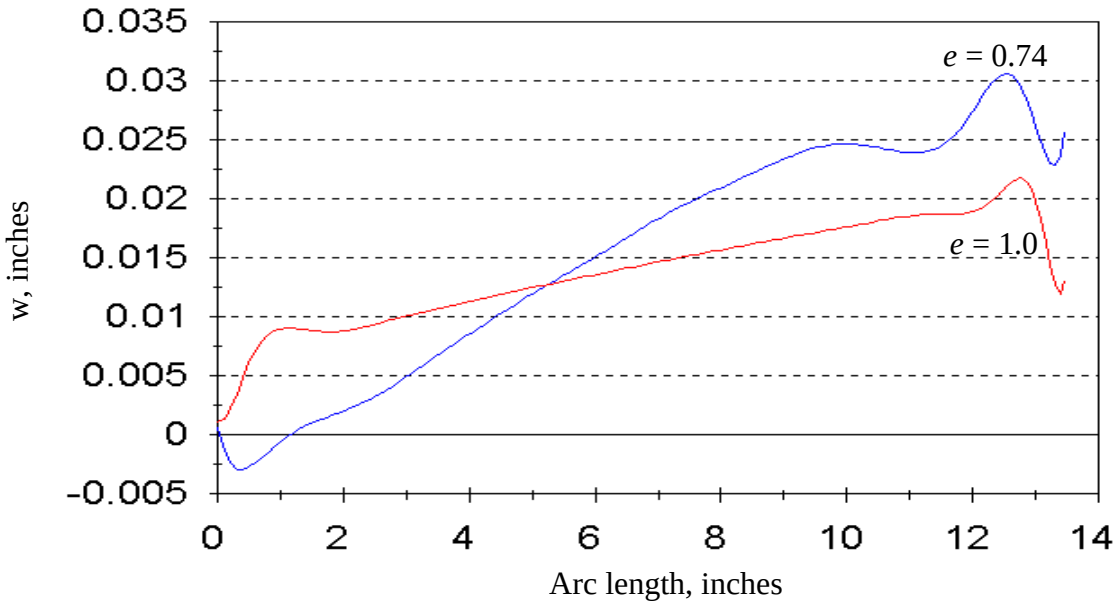

Fig. 6.6 Normal Displacement, Quasi-isotropic Dome

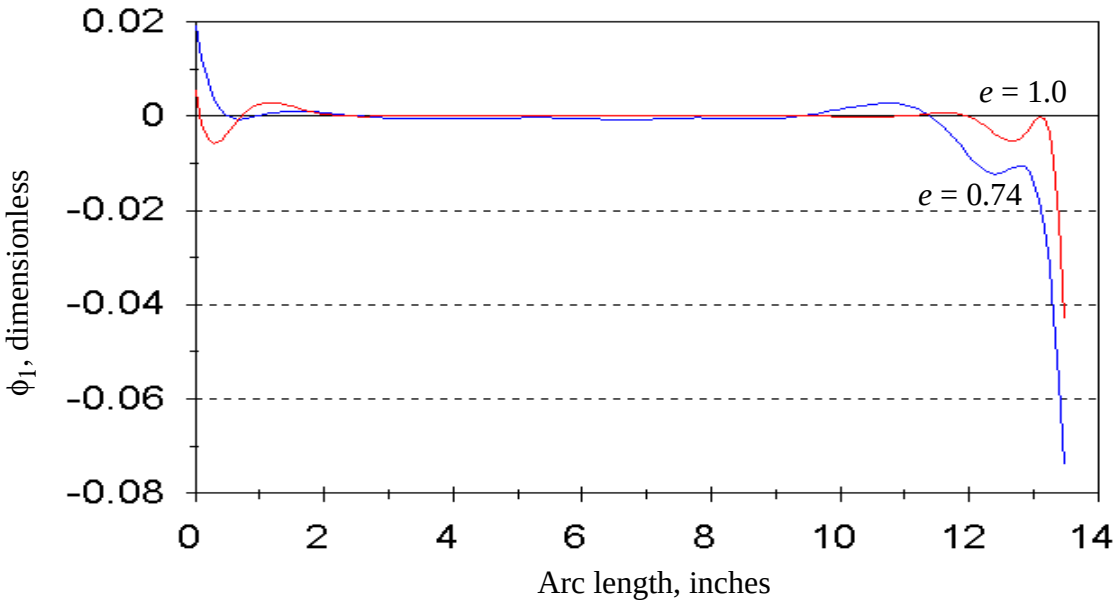

Fig. 6.7 Rotation about the Circumferential Axis, Quasi-isotropic Dome

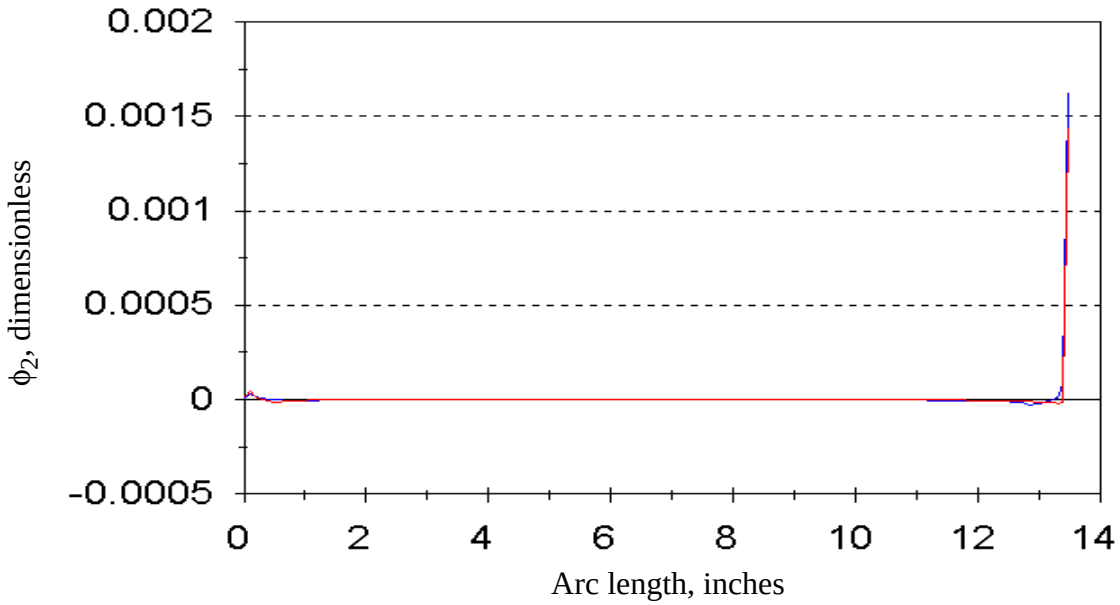

Fig. 6.8 Rotation about the Meridional Axis, Quasi-isotropic Dome

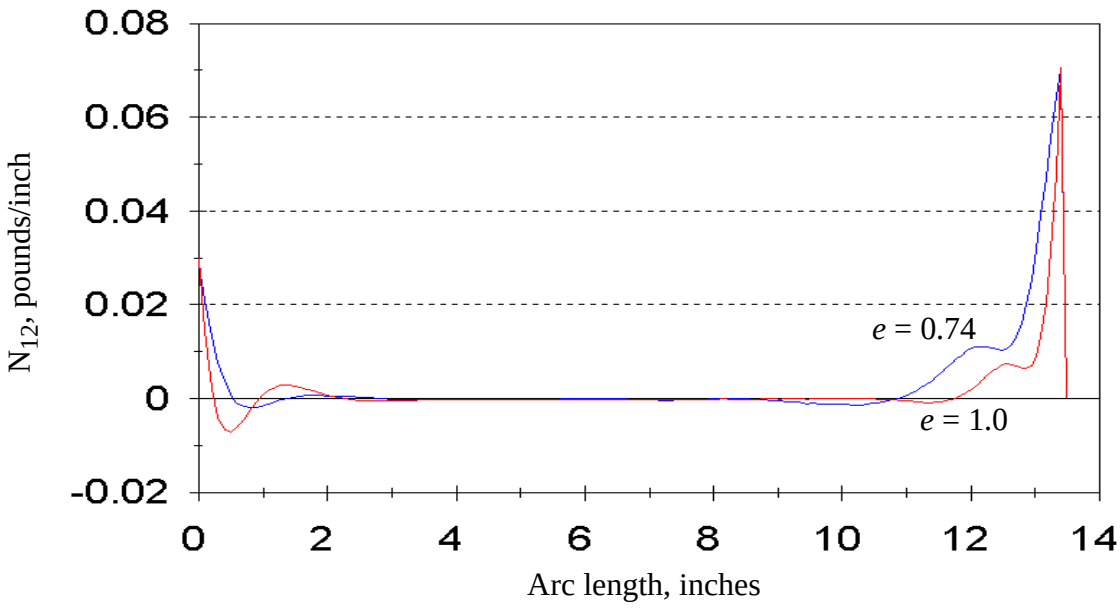

Fig. 6.9 In-plane Shear Stress Resultant, Quasi-isotropic Dome

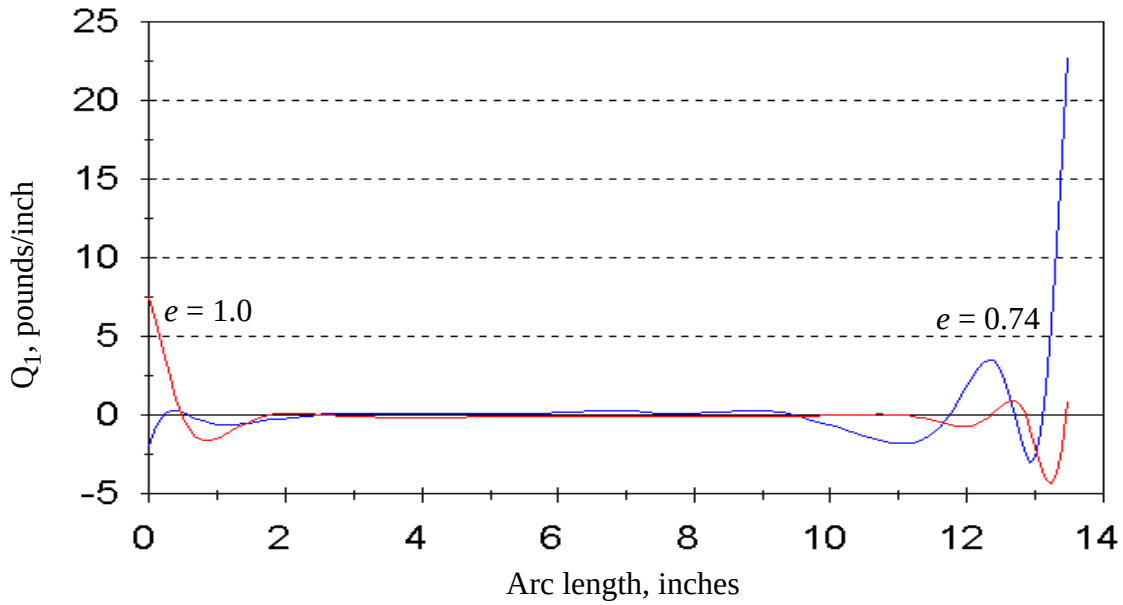

Fig. 6.10 Transverse Shear Stress Resultant on Meridional Face, Quasi-isotropic Dome

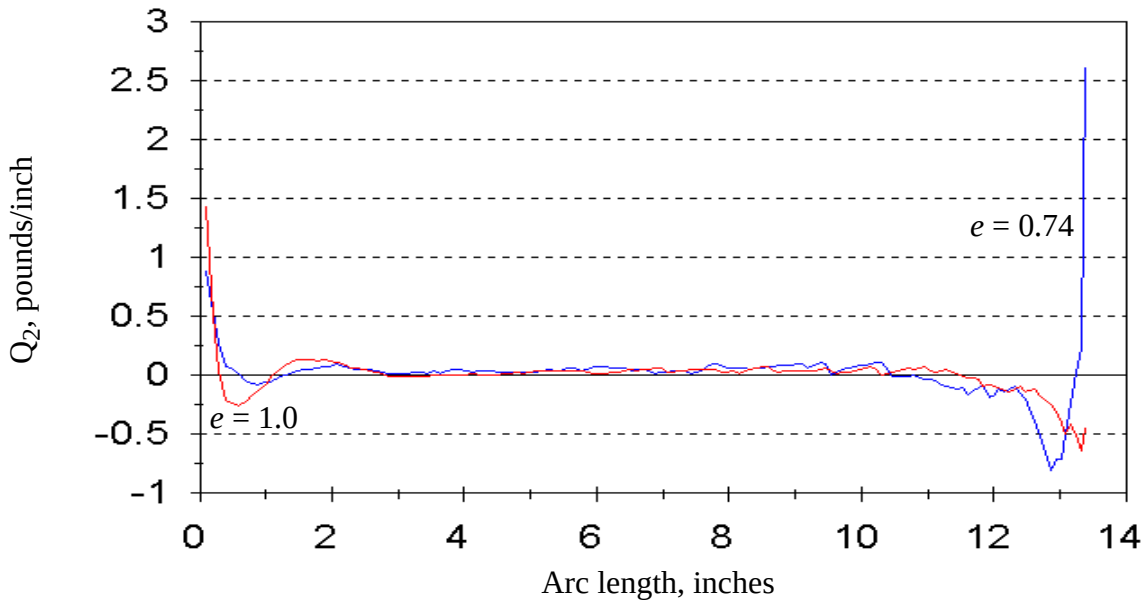

Fig. 6.11 Transverse Shear Stress Resultant on Circumferential Face, Quasi-isotropic Dome

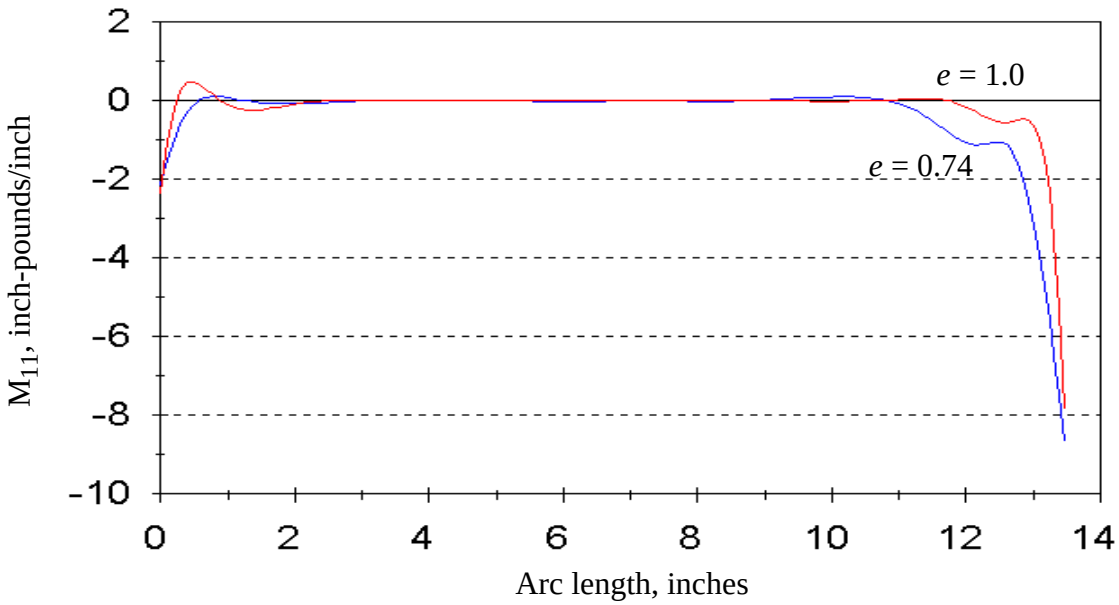

Fig. 6.12 Meridional Stress Couple, Quasi-isotropic Dome

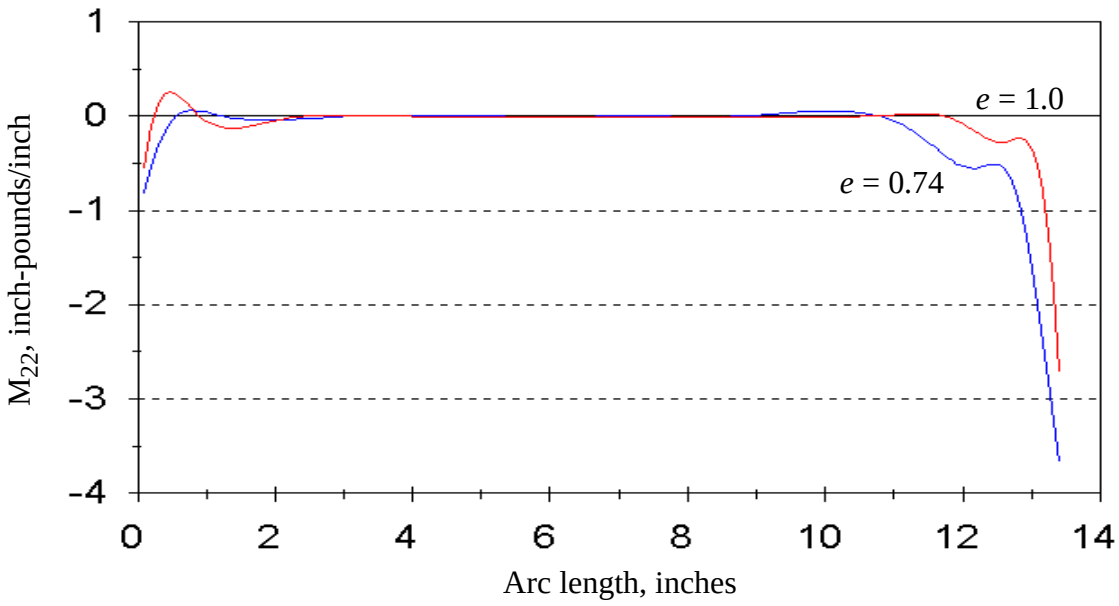

Fig. 6.13 Circumferential Stress Couple, Quasi-isotropic Dome

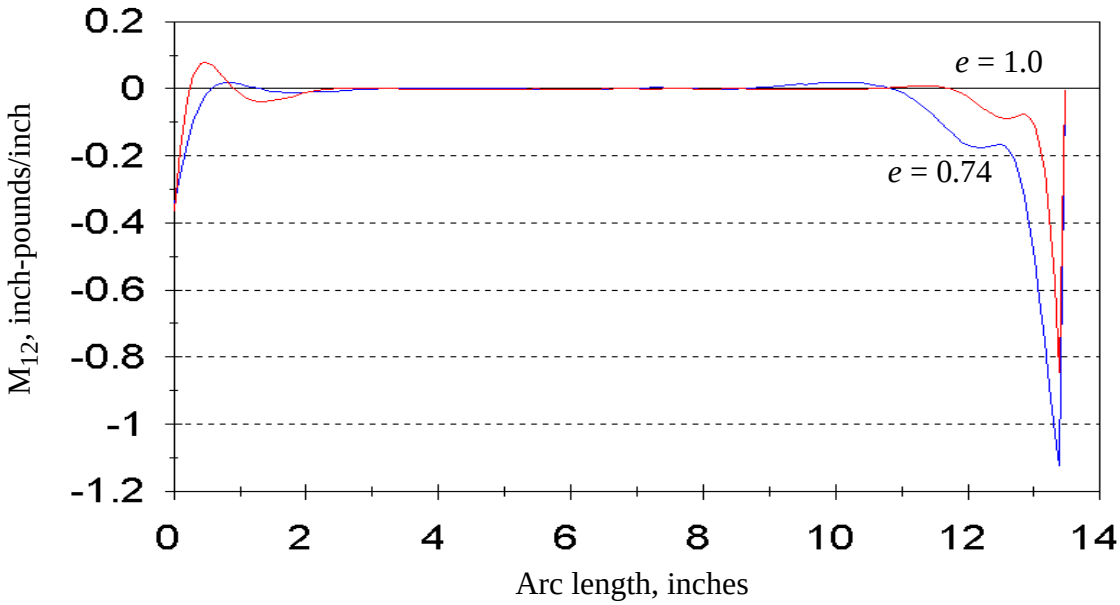

Fig. 6.14 In-plane Shear Stress Couple, Quasi-isotropic Dome

There are a few features of the figures above which bear some explanation. First, it will be noted in the plots of rotation about the meridian ϕ_2 (Fig. 6.8), and in-plane shear stress resultant and shear stress couple N_{12} and M_{12} (Figs. 6.9 and 6.14,respectively), there are "spikes" which appear in the vicinity of the cover plate joint. These are most likely mathematical artifacts which occur as a result of the assumed plate stiffness matrix. In particular, it was assumed that the plate provides no resistance against rotation ϕ_2, leading to the large ϕ_2 spike. In reality, it might be better to assume some nonzero stiffness against such a rotation.

In addition to the spikes in the output for the response variables noted above, there is another problem with the results presented here: the transverse shear stress resultant on the circumferential face Q_2 is somewhat poorly predicted, in the sense that the output is a bit noisy. Inasmuch as one of the goals of this work is to accurately predict the gradients of the transverse shear stress resultant, the noisiness of Q_2 is somewhat troubling. More work needs to be done to reduce this problem, but it is worth noting that the problem of noisy data is eliminated for the transverse shear stress resultant on the meridional face, Q_1, an advantage over the finite element

method. Also note that the calculation of Q_2 requires more accuracy in the description of the geometry than do the other secondary response quantities (N_{22}, M_{22}). Specifically, the formulation for Q_2 requires the third derivative of the radius, which is discontinuous in the cubic spline interpolation. The cubic spline interpolation only represents the geometry exactly for a spherical shell. Note from Fig. 6.11 that the spherical shell exhibits less waviness in the output for Q_2. The inaccuracy of the geometric description, combined with the spikes seen in some of the primary response quantities could explain the problems with Q_2. It is recommended that future implementations of this solution method use a more exact geometric representation.

There is also a small non-zero circumferential displacement predicted for the shell. This is likely a result of the $1/(1+\zeta/R)$ terms in the integrals for the generalized stiffness matrix. These ζ/R terms result in non-zero terms in the upper right and lower left quarters of the generalized stiffness matrix (the B_{ij} terms of equation (2.56)) which would be identically zero for a symmetrically laminated flat plate. Refer to equations (2.57). These non-zero terms arising from shell curvature mathematically couple tension and twist in the shell, resulting in the non-zero circumferential displacement demonstrated in Fig. 6.5.

In the interest of completeness, the study of dome ellipticity effects on the structural response was continued for ellipticities below $e = 0.73$. In the process it was seen that the shooting technique failed to converge for a ellipticity of $e \leq 0.65$. Failure to converge for increased ellipticity may be an indication of limit point buckling. As a test of this hypothesis, the pressure was lowered and convergence was again obtained at $e = 0.65$, for pressure between 53 and 54 psi. The shooting code as written does not contain checks on stability, but uses the load control method in the iterations for the nonlinear analysis. It is thus possible to attempt to increase loading beyond a limit point, into a regime where there is no possible solution to the state vector equations with the given boundary conditions. In that case, the method would naturally fail to converge. Thus, while the condition is not fully confirmed by the test just described, the result is consistent with what one might expect for limit point buckling.

6.3 Other ellipsoidal domes

The results of section 6.2 have suggested that the "best" geometry for an ellipsoidal dome with a quasi-isotropic layup has ellipticity of $e = 0.74$. In this section, we seek to determine whether a change in laminate layup might allow for a further improvement.

6.3.1 Meridionally stiff and circumferentially stiff laminates

Examination of the results of the previous section for quasi-isotropic domes reveals that the most limiting response quantity seems to be the circumferential stress resultant N_{22}. Specifically, the presence of compressive N_{22} is problematic. In this section, we examine whether dome material properties may be used to create a load transfer from the meridional to the circumferential direction, in order to relieve the hoopwise compressive state for ellipticity $e = 0.73$. To examine this quickly, we look at two layups, each found by reorientation of two plies of the quasi-isotropic laminate. Specifically, we look at $[\pm 45, 0_2]_s$ and $[\pm 45, 90_2]_s$ laminates. The first of these is preferentially stiffened in the meridional direction, and the second is stiffened in the circumferential direction. Refer to Fig. 6.15. Comparison of the response of the two new laminates to one another and to the quasi-isotropic case suggests that it is best to make the laminate stiff in the meridional direction, if it becomes necessary to utilize a non-quasi-isotropic laminate. It may also be seen, however, that both the meridionally stiff laminate and the circumferentially stiff laminate exhibit worse hoop compression than does the quasi-isotropic laminate. There thus appears to be no real utility in the selection of either a $[\pm 45, 0_2]_s$ laminate or a $[\pm 45, 90_2]_s$ laminate over a quasi-isotropic layup.

6.3.2 Symmetric angle ply laminates

In this section, we look at symmetric angle ply laminates of the class $[\pm\alpha]_{2s}$. The parametric study was performed beginning with a baseline design of $\alpha = 45$ degrees -- a $[\pm 45]_{2s}$ layup. Subsequent analyses were performed for higher and lower values of α. In each case, the response was sequentially calculated beginning with an ellipticity $e = 1.0$, and proceeding to reduce e until a state of hoop compression was reached anywhere within the span of the dome meridian.

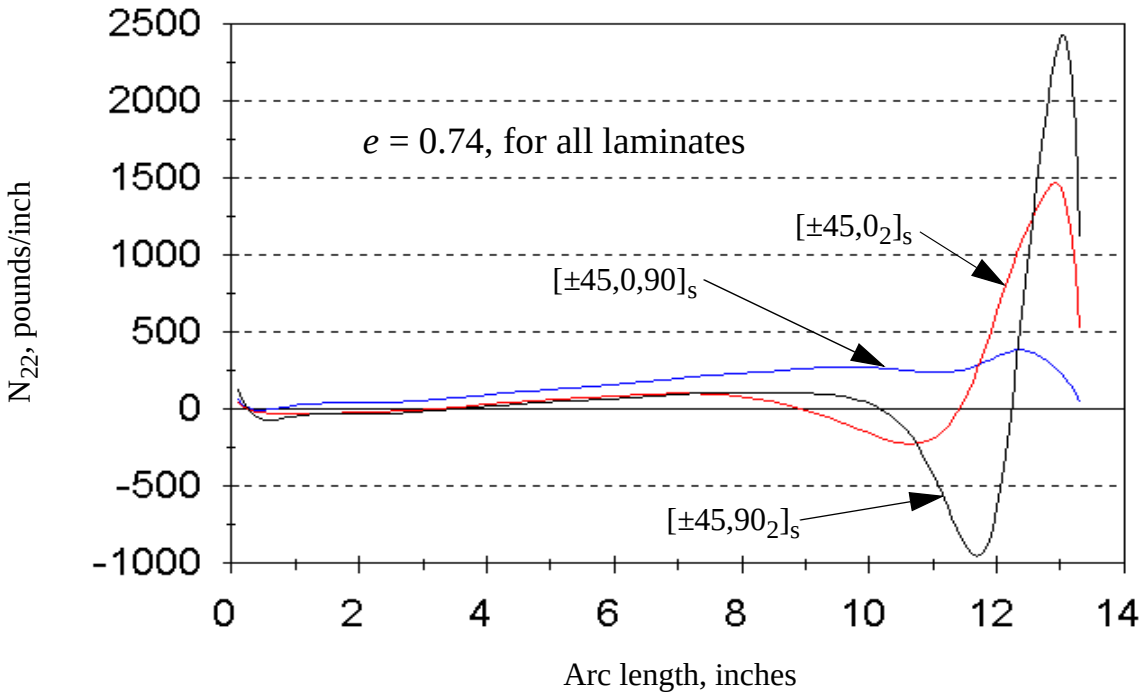

Fig. 6.15 Circumferential Stress Resultant, $[\pm 45,0_2]_s$ and $[\pm 45,90_2]_s$ laminates

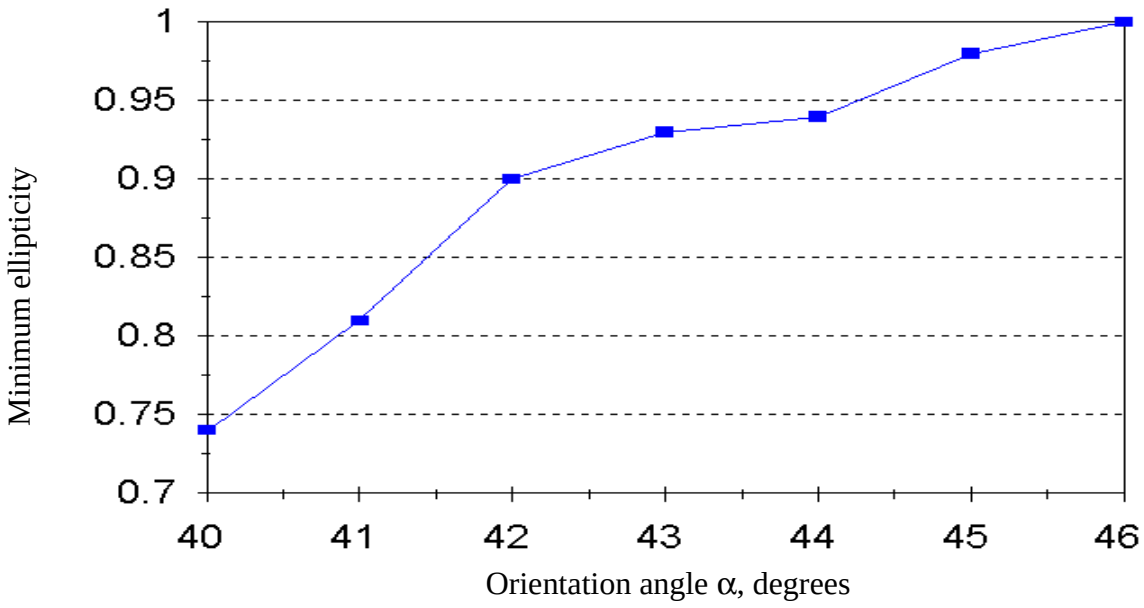

Fig. 6.16 Minimum Ellipticity vs. Orientation Angle, $[\pm\alpha]_{2s}$ laminates

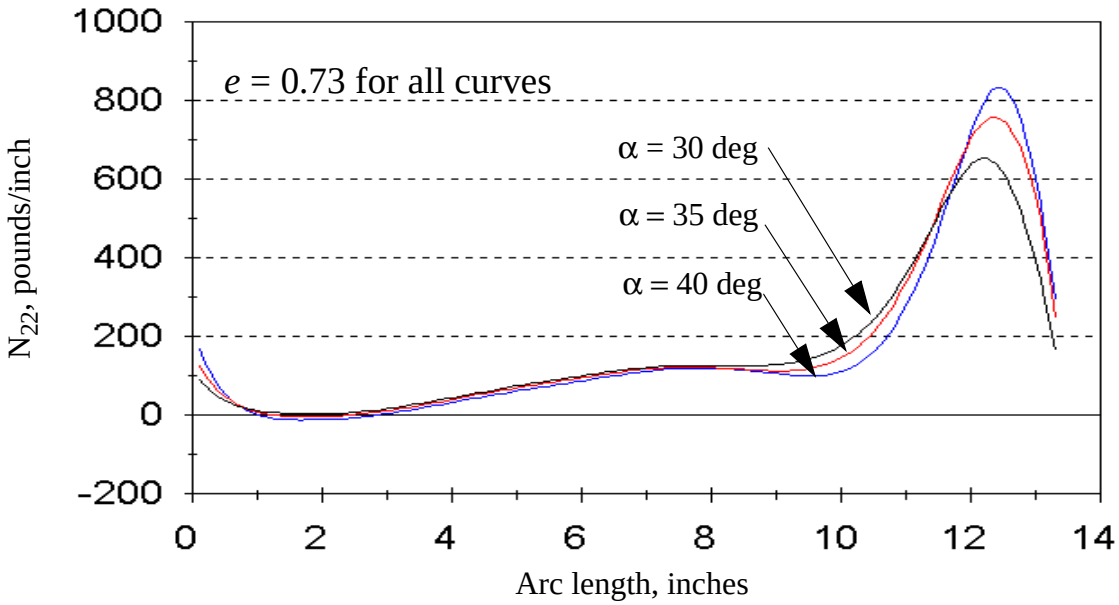

Fig. 6.17 Circumferential Stress Resultant, $[\pm\alpha]_{2s}$ Laminates

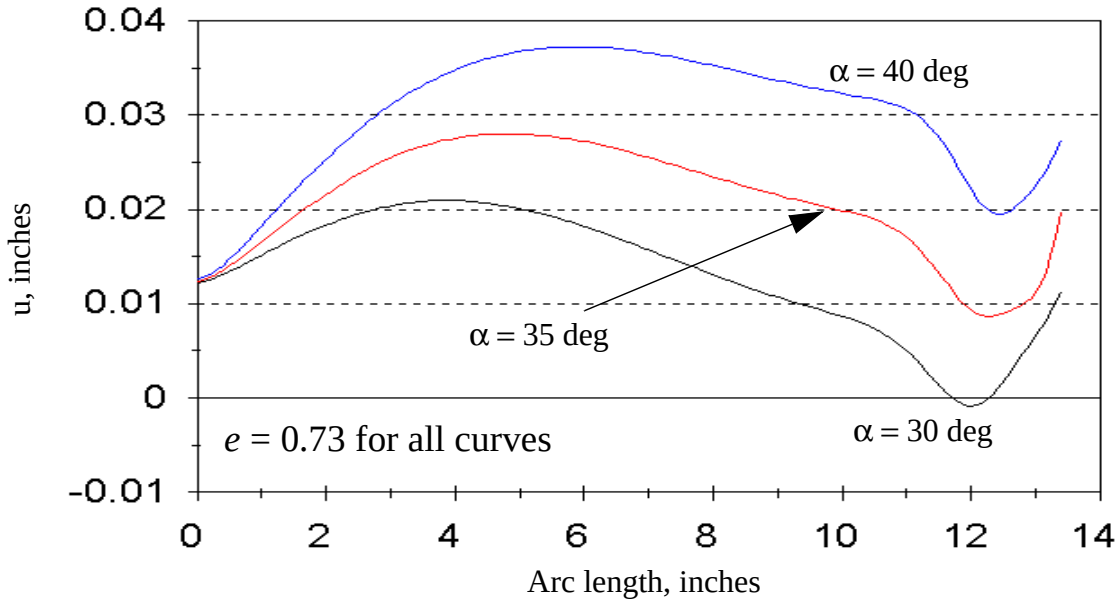

Fig. 6.18 Meridional Displacement, $[\pm\alpha]_{2s}$ Laminates

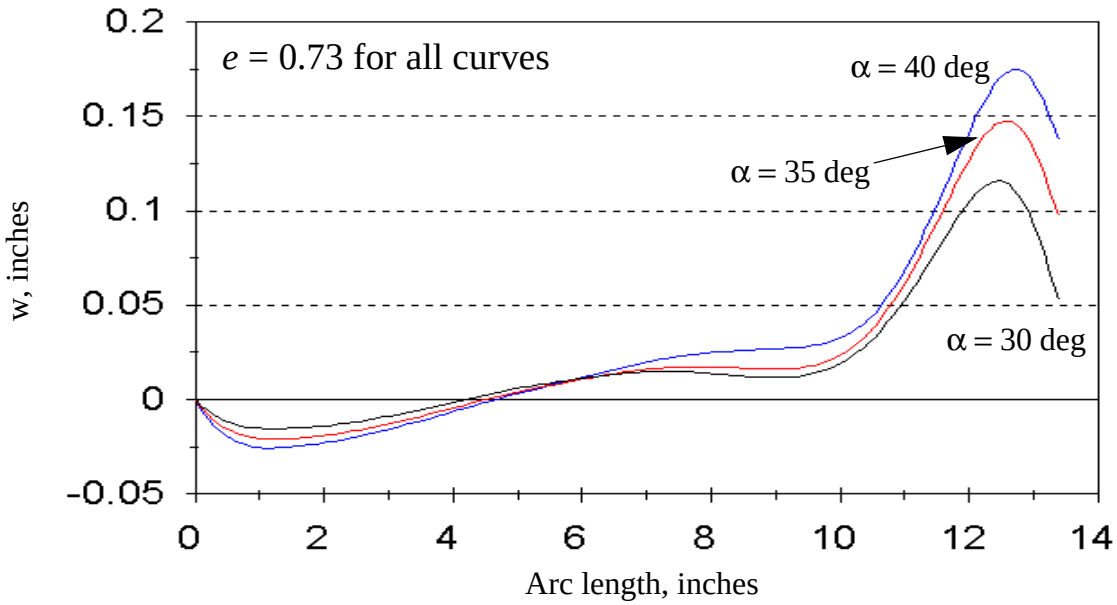

Fig. 6.19 Normal Displacement, $[\pm\alpha]_{2s}$ Laminates

It was seen in section 6.3.1 that preferential stiffening in the circumferential direction by adjustment of laminate stacking sequence is sometimes unwise (Fig. 6.15). Such a conclusion also is borne out here: it is better from the standpoint of overall structural response to have a stacking sequence which produces relatively high stiffness in the meridional direction, rather than having a laminate which is stiff in the circumferential direction, for ellipticity $e \le 1.0$. In fact, the results of this portion of the parametric study reveal that it is *impossible* to stiffen in the circumferential direction and at the same time flatten the dome, without inducing hoop compression. The minimum value of ellipticity e which may be used for $\alpha = 46°$ without hoop compression is $e = 1.0$. For orientation angles $\alpha = 47°$, $\alpha = 48°$, hoopwise compression is experienced even for the spherical geometry, and for ply orientation $\alpha = 50°$, the shooting method fails to converge at all. On the other hand, reduction in the angle α results in minimum values of ellipticity as shown in Fig. 6.16, for orientations down to 40 degrees. Note that the angle $\alpha = 40°$ has minimum ellipticity $e = 0.74$, the same as the "best" value for the quasi-isotropic dome. Reducing the ply orientation beyond 40 degrees has little additional effect; it is not until the angle α

approaches 30 degrees that the ellipticity can be further reduced. Some representative plots of the response for the orientation angles $\alpha = 30°, 35°, 40°$ are given in Figs. 6.17 - 6.19, for $e = 0.73$. It may be seen by examination of these figures that the overall response of the dome is made less severe than it would otherwise be, by aligning the fibers more closely with the meridian. On the other hand, orienting the fibers along the meridian produces a laminate which is very weak in the circumferential direction. In general, some preferential stiffening in the meridional direction seems to be a good idea, but it is possible to take the notion too far.

The results depicted in Figs. 6.17 - 6.19 show that a better overall response is had, among $[\pm\alpha]_{2s}$ laminates, for meridionally stiff cases; the following figures further reinforce this conclusion, and provide a basis for comparison between the $[\pm\alpha]_{2s}$ and $[\pm 45,0,90]_s$ laminates.

In general, it appears that the response of the quasi-isotropic dome is superior to the response of the symmetric angle-ply laminates, in the sense that the displacements of the angle-ply laminates are (relatively) huge. In Fig. 6.20, the displacements for the quasi-isotropic dome are scaled up by a factor of 50, while the displacements of the $[\pm 30]_{2s}$ dome are scaled up by a factor of 10. Even so, the displacements for the angle-ply dome appear much greater. In addition to the relatively huge displacements displayed by the symmetric angle ply laminates, as shown in Figs. 6.20 - 6.25, it may be seen that the stress resultants and stress couples are also higher for the symmetric angle-ply domes.

Note that the encoded check on fiber stress does not indicate any fiber failures for any of these cases, but even so there appears to be no utility in the use of symmetric angle-ply laminates instead of quasi-isotropics.

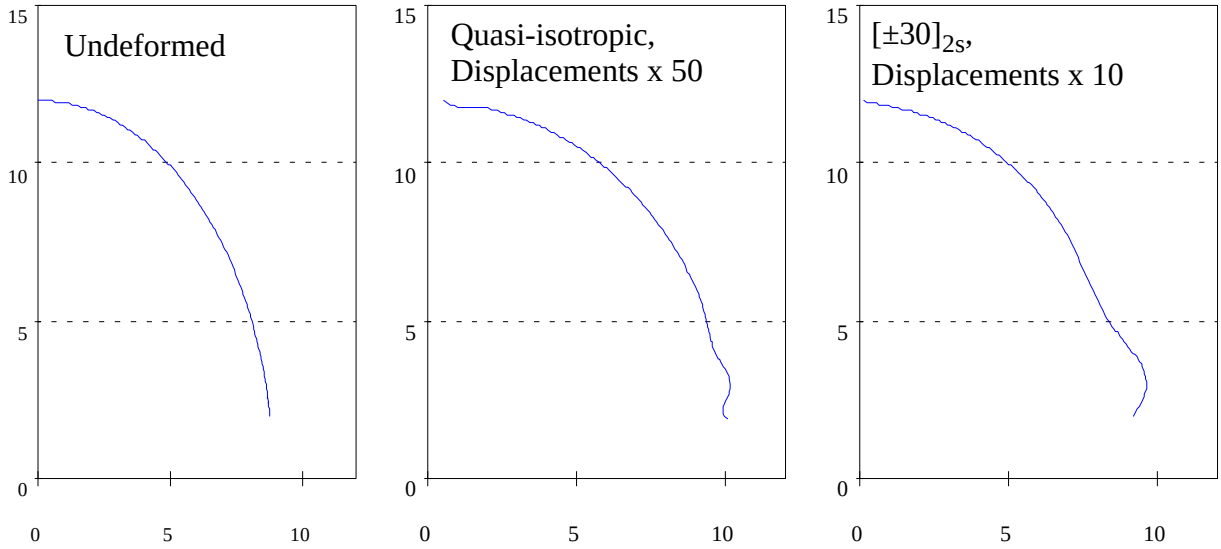

Fig. 6.20 Undeformed and Deformed Meridians, Ellipticity e = 0.74

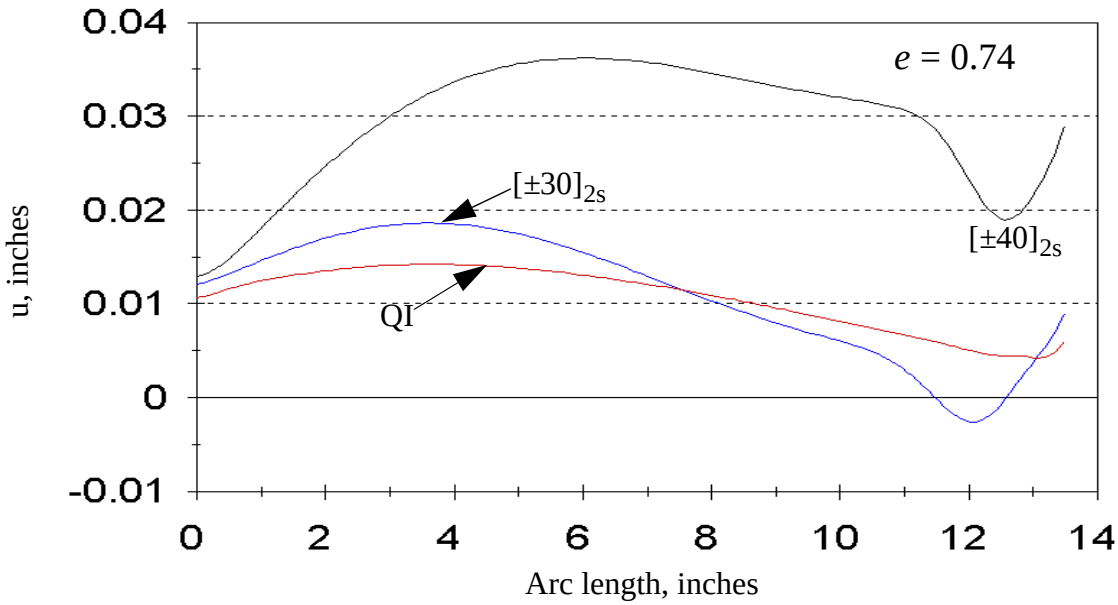

Fig. 6.21 Meridional Displacement, Quasi-isotropic vs. Angle-ply Laminates

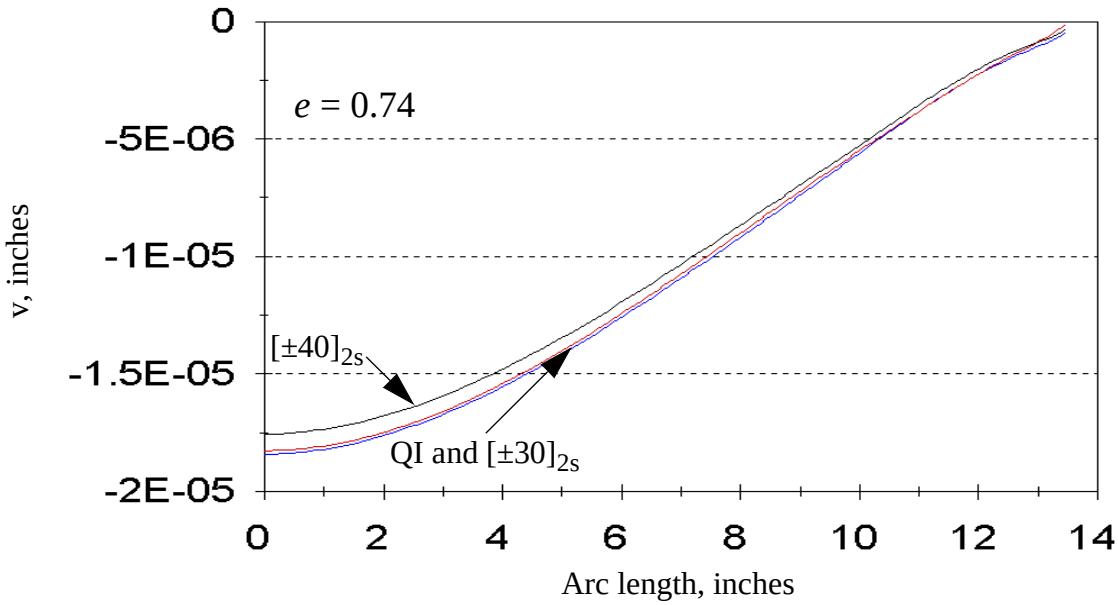

Fig. 6.22 Circumferential Displacement, Quasi-isotropic vs. Angle-ply Laminates

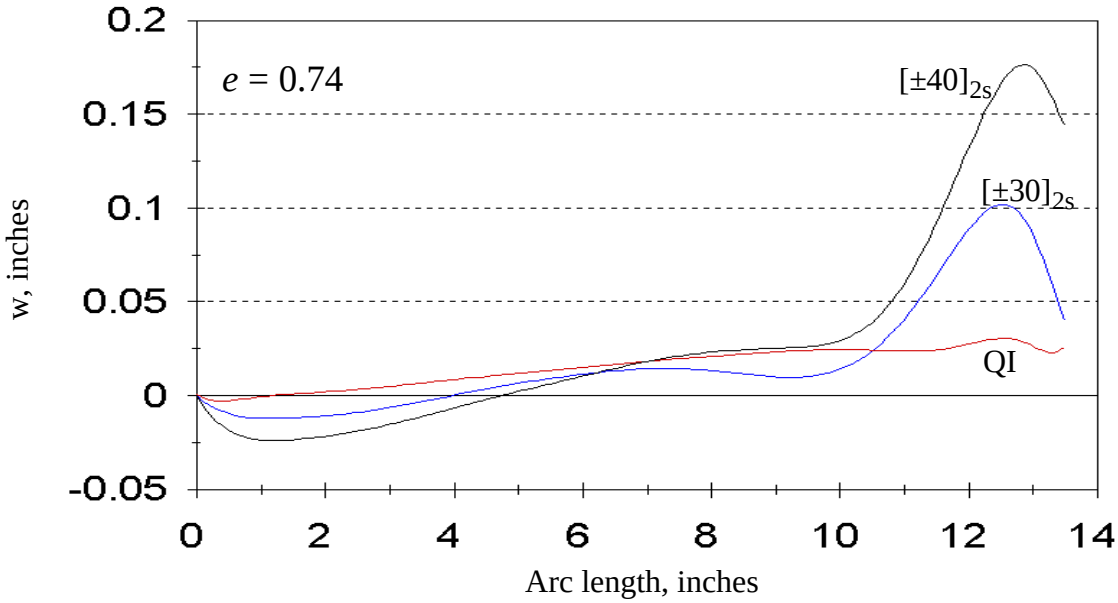

Fig. 6.23 Normal Displacement, Quasi-isotropic vs. Angle-ply Laminates

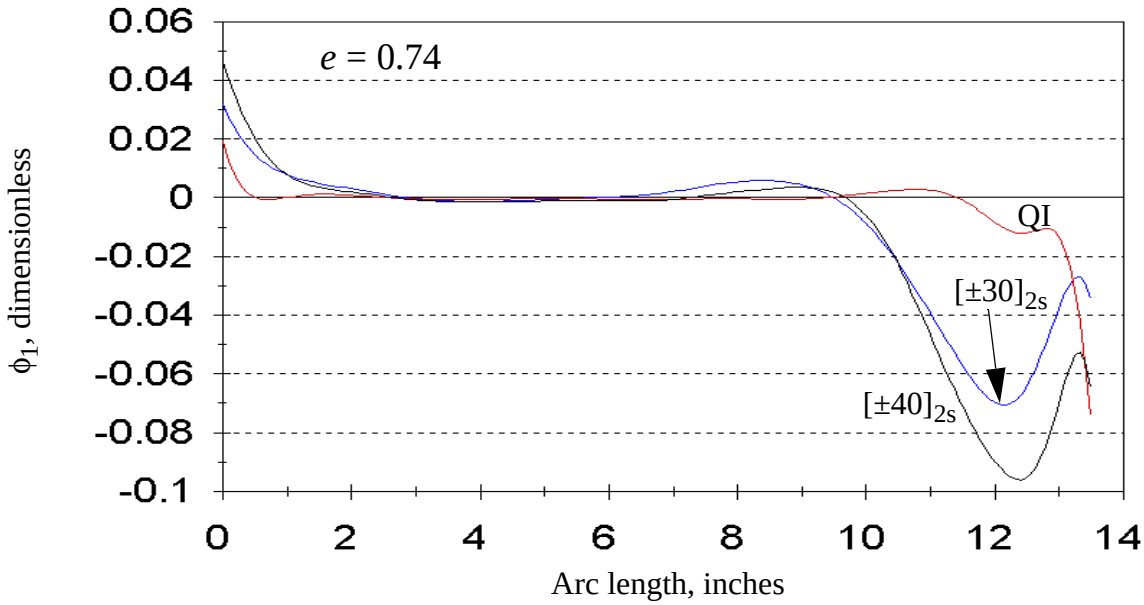

Fig. 6.24 Rotation about the Circumferential Axis, Quasi-isotropic vs. Angle-ply Laminates

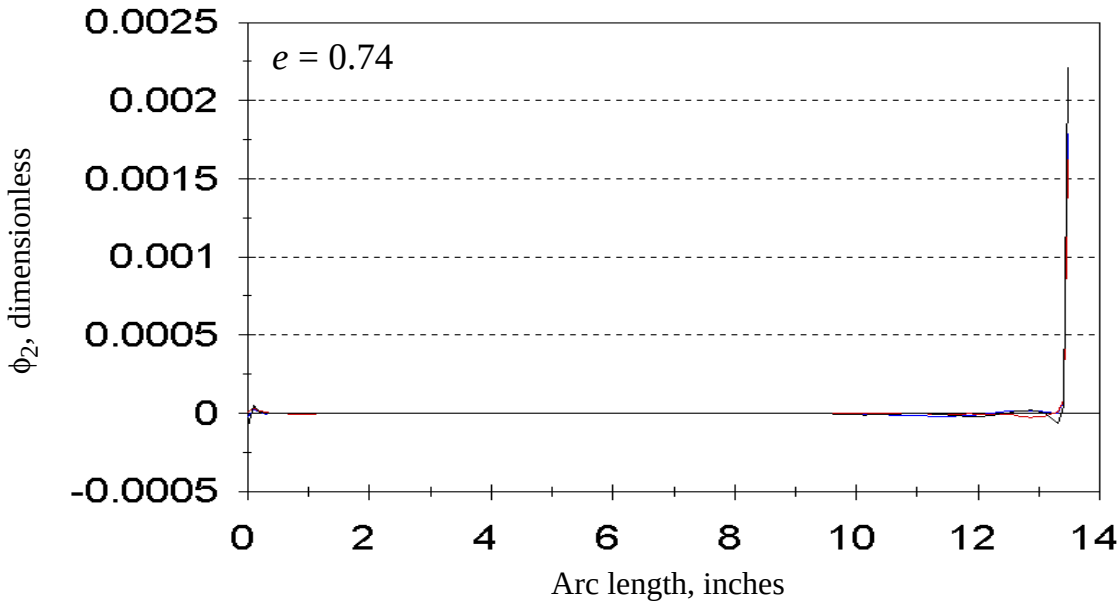

Fig. 6.25 Rotation about the Meridional Axis, Quasi-isotropic vs. Angle-ply Laminates

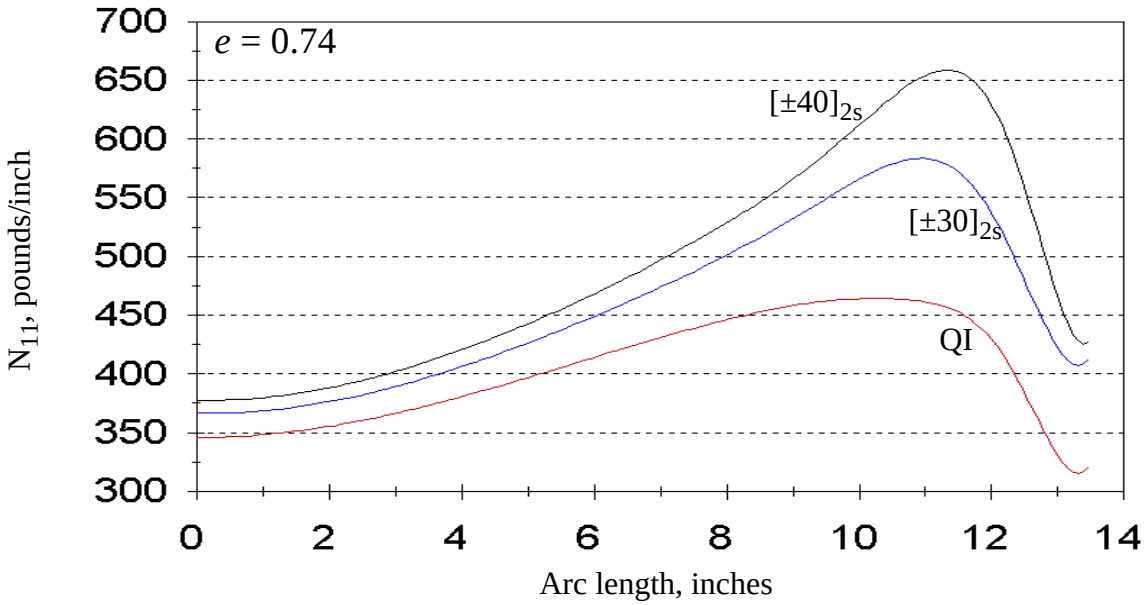

Fig. 6.26 Meridional Stress Resultant, Quasi-isotropic vs. Angle-ply Laminates

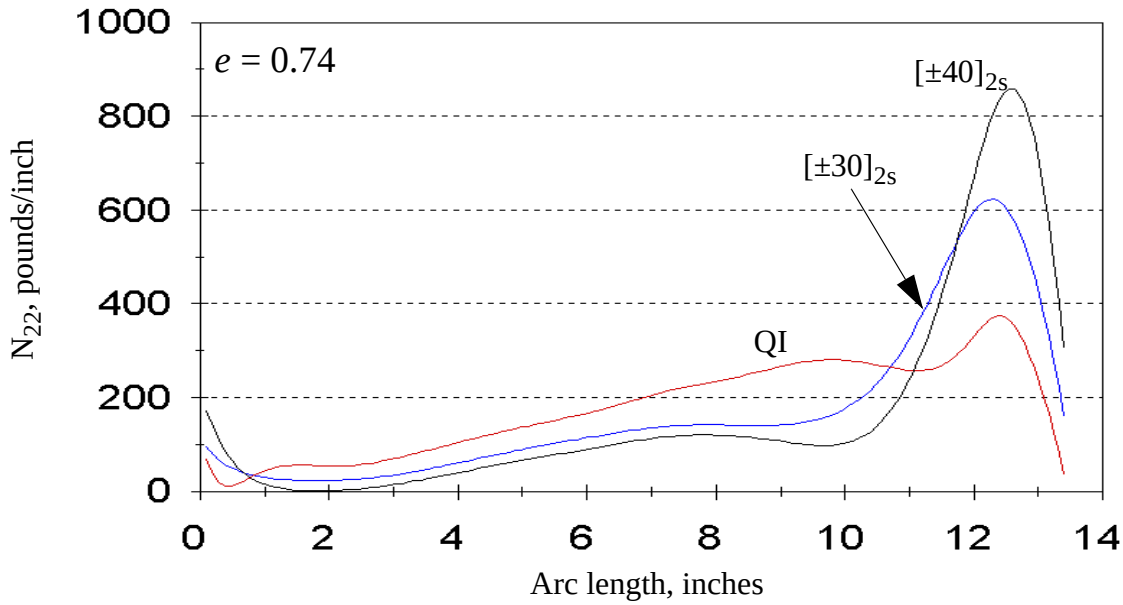

Fig. 6.27 Circumferential Stress Resultant, Quasi-isotropic vs. Angle-ply Laminates

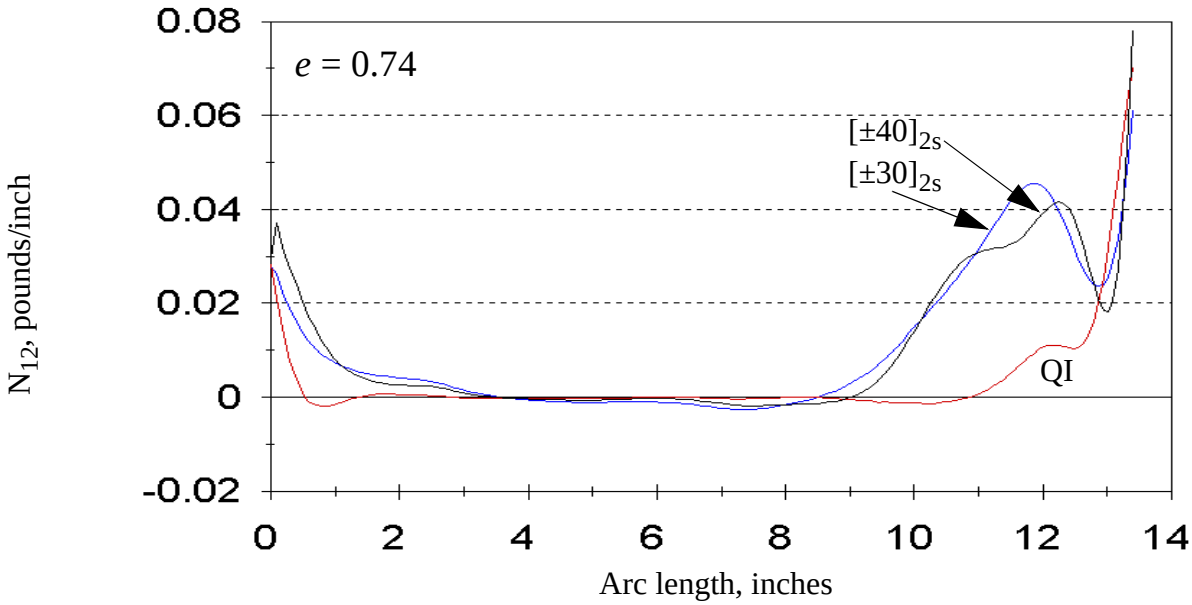

Fig. 6.28 In-plane Shear Stress Resultant, Quasi-isotropic vs. Angle-ply Laminates

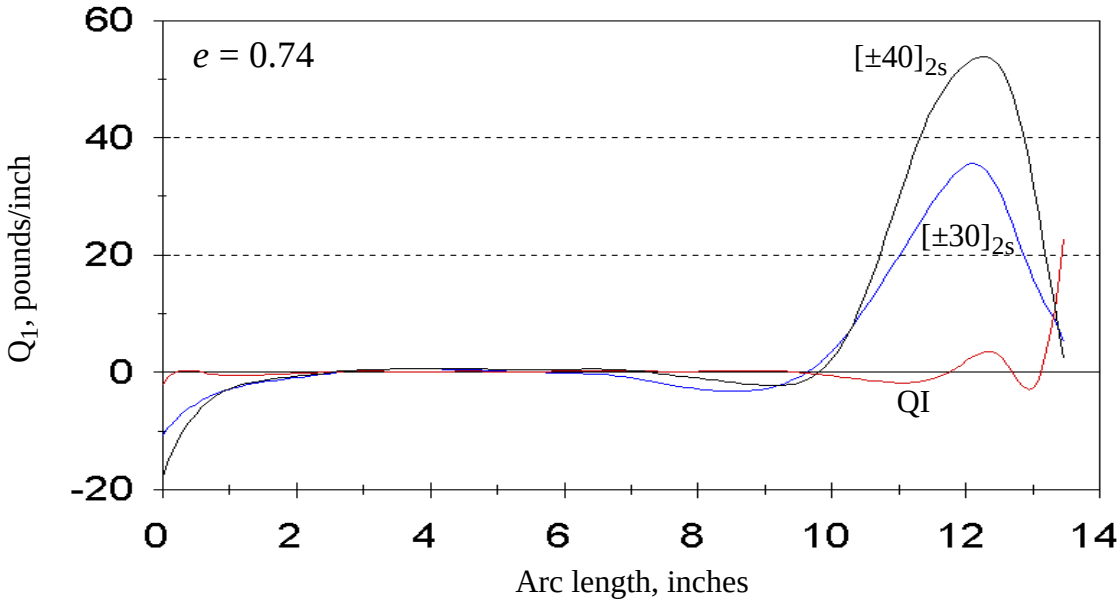

Fig. 6.29 Transverse Shear Stress Resultant Q_1, Quasi-isotropic vs. Angle-ply Laminates

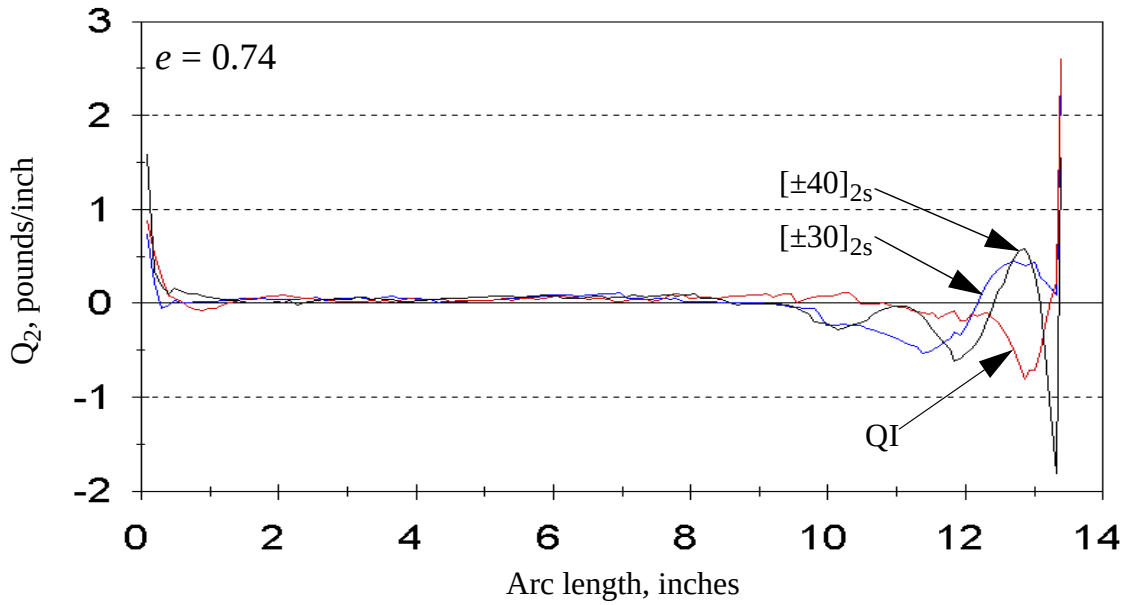

Fig. 6.30 Transverse Shear Stress Resultant Q_2, Quasi-isotropic vs. Angle-ply Laminates

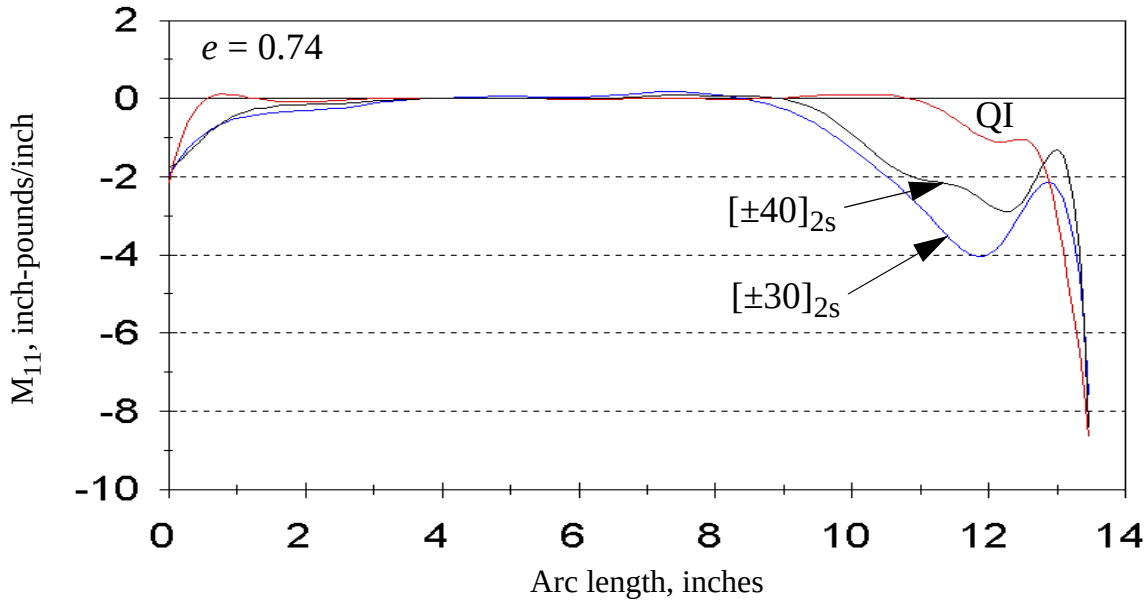

Fig. 6.31 Meridional Stress Couple, Quasi-isotropic vs. Angle-ply Laminates

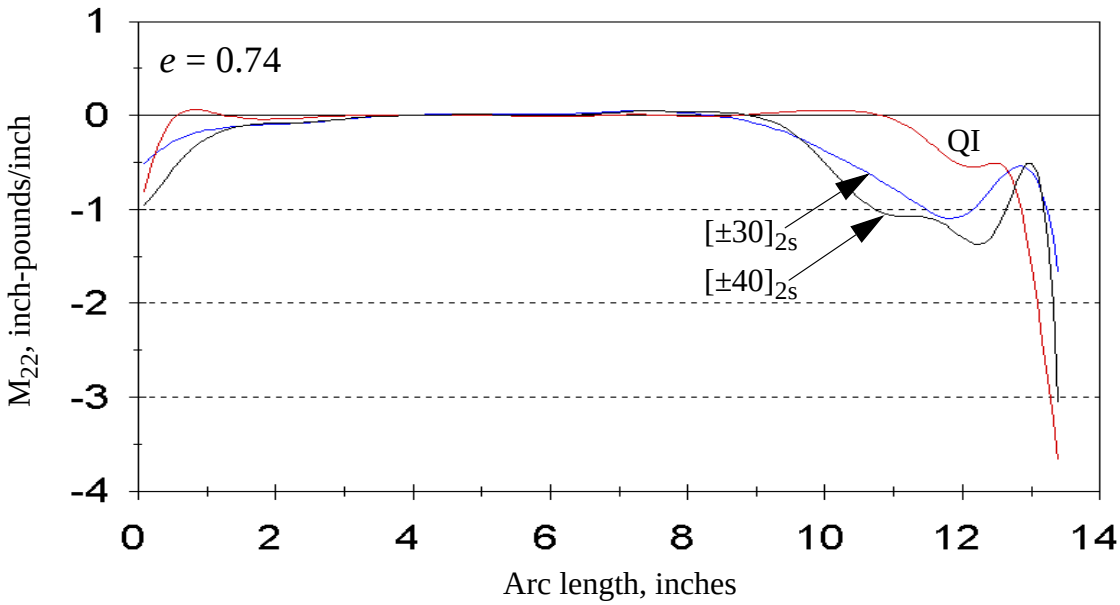

Fig. 6.32 Circumferential Stress Couple, Quasi-isotropic vs. Angle-ply Laminates

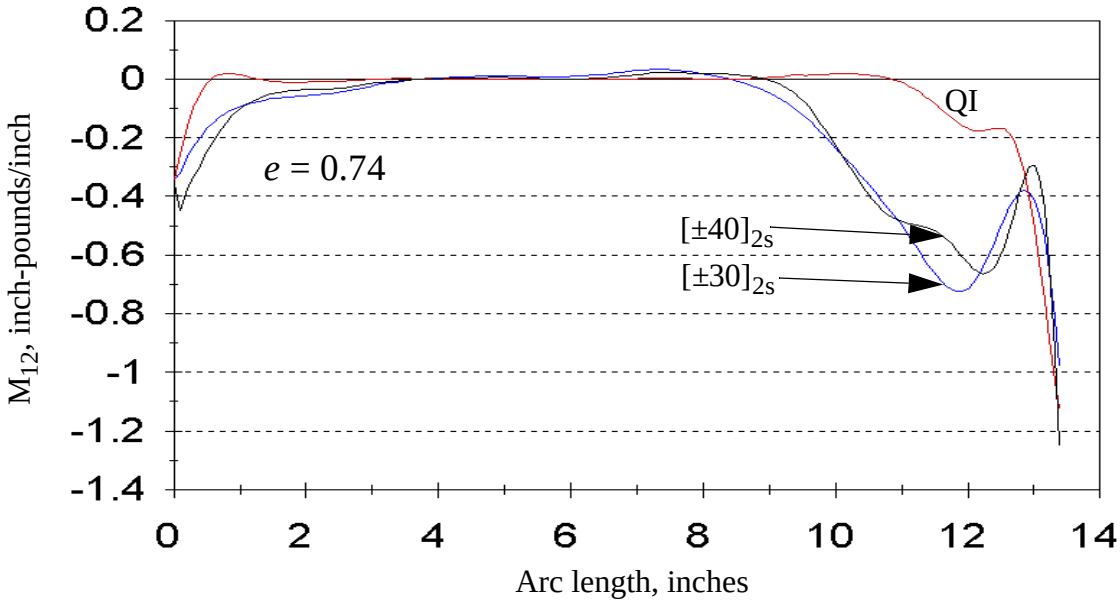

Fig. 6.33 In-plane Shear Stress Couple, Quasi-isotropic vs. Angle-ply Laminates

While the conclusion of the above analysis may be that there is no particular advantage to the use of the symmetric angle-ply laminate over the quasi-isotropic laminate, there may yet be an advantage in the choice of the quasi-isotropic laminate over the metallic dome. Refer to Fig.1.1. It may be noted that the metallic dome requires a good many meridional stiffeners. These occur as a necessary result of the construction process. The metal dome is formed by joining together many triangular pieces, each joint then needing a stiffener to hold it together. These stringers must make up a significant portion of the dome weight, and might be eliminated in the case of a laminated dome, which may be constructed by filament winding or by tow placement.

6.4 A word about the effect of cover plate geometry

It was argued in section 6.2 that such boundary layer effects as occur for quasi-isotropic ellipsoidal domes are primarily resultant from geometric and material discontinuity at the dome/ cover plate interface. To examine the veracity of that argument, we adjusted plate geometry for a quasi-isotropic dome, ellipsoidal with $e = 0.73$, and noted the resultant effects on the overall structural response of the dome. We used a baseline plate geometry as has been used all along for this study: three inch radius, with 0.04 inch thickness, titanium alloy. Adjustments to this geometry were made to examine alternate cover plate designs, which differed from the baseline in radius and thickness. The quality of the response of the dome in each case was judged by the magnitude of the compressive hoop stress resultant. We first reduced the cover plate radius to two inches, while maintaining the 0.04 inch thickness. This had a slight beneficial effect on hoop compression. We next doubled the plate thickness, at two inch radius; this made hoop compression worse. Following this, we increased plate radius to four inches, and analyzed for 0.08 inch thickness and 0.04 inch thickness. In both cases, hoop compression was made worse, rather than better. In short, the conclusion to be drawn from this very rudimentary numerical experiment is that the "best" design for the cover plate is that which has minimum radius, to reduce the geometric discontinuity, and thickness chosen to minimize the material discontinuity. That is, the results suggest that the best cover plate, in terms of dome response, is none at all. For manufacturing purposes, the cover plate is necessary; it should merely be designed to have minimal radius. The assertion of section 6.2 regarding discontinuity at the cover plate thus seems to be borne out.